NBSIR 75-658

Electron Microscopic Observations of Microcracking About Indentations in Aluminium Oxide and Silicon Carbide

B. J. Hockey and B. R. Lawn

Inorganic Materials Division
Institute for Materials Research
National Bureau of Standards
Washington, D. C. 20234

January 1975

Interim Report for Period July 1, 1974 through June 30, 1975

Prepared for
Department of the Navy
Office of Naval Research
Arlington, Virginia 22217

NBSIR 75–658

ELECTRON MICROSCOPIC OBSERVATIONS OF MICROCRACKING ABOUT INDENTATIONS IN ALUMINIUM OXIDE AND SILICON CARBIDE

B. J. Hockey and B. R. Lawn

Inorganic Materials Division
Institute for Materials Research
National Bureau of Standards
Washington, D. C. 20234

January 1975

Interim Report for Period July 1, 1974 through June 30, 1975

Prepared for
Department of the Navy
Office of Naval Research
Arlington, Virginia 22217

U. S. DEPARTMENT OF COMMERCE, Frederick B. Dent, Secretary

NATIONAL BUREAU OF STANDARDS, Richard W. Roberts, Director

1. Introduction

Indentation hardness testing is finding an increased usage in the scientific investigation of damage processes in highly brittle solids [1]. A suitably sharp indenter tip concentrates very high levels of stress, particularly in shear and hydrostatic compression, and thus induces irreversible deformation in conveniently localized regions of a test surface. In many brittle materials the mean contact pressure can be as much as a tenth of an elastic modulus [2], indicating that the intrinsic bond strength of the lattice itself must surely be exceeded in places. Despite a recent proliferation of indentation damage studies, the exact nature of such irreversible deformation processes in brittle solids remains something of a contentious issue.

One aspect of indentation damage which has been largely overlooked is that of indentation-induced cracking. In the general indentation field a component of tension, however small, is unavoidable [3], and there is a growing body of evidence suggesting that cracking may be more prevalent than one might have been led to believe from earlier studies. An understanding of indentation fracture is important for many practical as well as academic reasons (for a review see [4]): a pertinent example is strength degradation as a result of particle-surface contact, where individual damage events may be usefully simulated in a standard hardness testing device.

The chief object of this work is to report on observations of microcrack patterns about small-scale point indentations in aluminium oxide and silicon carbide, two highly brittle materials currently of great interest in ceramics engineering. The results represent part of a detailed study of residual crack interfaces using transmission electron microscopy. Our emphasis here is directed to geometrical features of the observed crack interfaces. The observed crack geometry is discussed in terms of an earlier proposal for crack growth beneath sharp indenters based on optical observations [3]. The study complements an analysis of diffraction contrast effects at large-scale remnant cone cracks in sphere-indented silicon using X-ray topography [5].

2. Preparation of Indentation Specimens for Electron Microscopy

The method of specimen preparation was similar to that previously described [6-8]. Single crystals of sapphire and α-silicon carbide were cut into slabs and polished, first mechanically and then chemically, to a thickness of about 100 μm. Indentations were made with either a Knoop or Vickers diamond pyramid at a load of 200 g on each test surface. An optical examination of the surfaces showed clear evidence of microcracking in most cases, especially about the Vickers indentations. The crystals were then thinned to a size suitable for 200 kV transmission electron microscopy by ion bombardment [7]. Most of the material removed was from the surface below the indentation, although a little ($\approx$1μm) was removed from the top surface as well to eliminate any spurious damage incurred in specimen handling.

The bulk of the foils examined were prepared at room temperature. However, a few were subjected to prescribed thermal or mechanical

treatments between the indentation and thinning stages, as described in [8]. About one-hundred indentations in sapphire, and about twenty-five in silicon carbide, were investigated in this way.

3. Electron Microscopy of Cracks

3.1 General crack morphology

Intense diffraction contrast was observed in the immediate vicinity of all impressions. At the edges of the impressions, the images of dislocations, and sometimes of twins as well, could be clearly resolved. An analysis of this deformation has been given in the case of sapphire in an earlier paper [7], and similar deformation patterns have recently been analysed in indented silicon [9,10]. The diffraction spot pattern was maintained at all locations in the foils, although considerable broadening of the spots was evident in the most heavily deformed regions. No diffraction evidence was found for any crystallographic phase transformation resulting from the indentation process.

Cracking was observed about all Vickers impressions examined, and about most Knoop impressions. With the Vickers specimens, cracks were always observed to extend radially outward from the corners of the indentations, their plane oriented very nearly normal to the foil surfaces, as seen clearly in Fig. 1 (silicon carbide). In addition, cracks lying nearly parallel to the foil surfaces were often observed between the radial cracks, again as in Fig. 1, but the geometry and indeed the frequency of appearance of this type of crack were sporadic. In the case of Knoop specimens, for example Fig. 2 (sapphire), the incidence of

detectable radial cracking was considerably less than for Vickers specimens, but for the lateral type of cracking the incidence was almost the same.

These observations may be readily explained in terms of the scheme for crack growth beneath sharp indenters put forward by Lawn and Swain [3]. Basically, two distinct stages of crack formation are apparent. The first occurs on indenter loading; at some (low) threshold level of stress a crack initiates at the deformation zone immediately below the sharp point of the indenter and extends downward on a plane of symmetry containing the contact axis. Fig. 3 depicts schematically the shape of this crack, the so-called "median vent crack," in its well-developed form. Diagram (a) indicates how the thinned foil samples the crack about the deformation zone. The median vents accordingly appear as ribbon-like segments along the lines of greatest stress concentration, as depicted in (b) for the Vickers and (c) for the Knoop specimens respectively. It is clear that the shape of the remnant crack will not be too sensitive to the exact location of the foil with respect to the original indented surface. The second stage of crack formation occurs on unloading; just prior to removal of the indenter new cracks initiate at the deformation zone and extend sideways into a shallow saucer-shaped configuration, modified to some extent by the presence of the median vents. This crack, the "lateral vent", is depicted in Fig. 4. In this case the location of the foil becomes a critical factor; small changes in the relative amounts of material removed from the upper and lower surfaces of the indented

crystal during thinning might result in the loss of a portion, if not all, of the lateral vent system. One further, very important consideration in connection with the geometry of remnant lateral vents is the axis of loading; in practice it is no easy matter to ensure near-perpendicularity between indenter axis and specimen surface, and preferred cracking on one side of the indentation tends to be the rule rather than the exception. In Fig. 5 we indicate how such asymmetry accounts for the apparently complex crack morphology seen in the electron micrograph of Fig. 2.*

3.2 Interfacial fringe and dislocation contrast

An examination of the diffraction contrast of the remnant cracks provides quantitative evidence for residual lattice mismatch across the interfaces. Essentially, the crack images are typified by fringe and dislocation networks. Figs. 6 and 7, showing median vents about Vickers indents in silicon carbide and sapphire respectively, and Figs. 8 and 9, showing lateral vents about a Vickers indent in silicon carbide and a Knoop indent in sapphire respectively, are examples. The patterns in all cases are largely characteristic of mismatch contrast [11, 12], generated by interference between slightly mismatched, simultaneously diffracting portions of crystal across the crack interfaces, although there is some indication of thickness fringe modulation where the interface is inclined to the foil surface (e.g. Fig. 7). This diagnosis was confirmed by observing the spacing of the fringes to remain invariant with voltage of the electron beam in the microscope (e.g. by lowering from 200 kV to 100 kV) [11].

---

*A distinct example of such asymmetry in crack pattern due to inclined loading of a Knoop indenter on a quartz surface may be seen in Fig. 7 of Ref. [3].

Fringe patterns of the mismatch type associated with residual cavities or cracks may be categorised into either displacement or moiré systems [12]. The displacement system is generated when the opposing crystal portions are separated by a rigid-body displacement $\underset{\sim}{c}(\underset{\sim}{r})$, where $\underset{\sim}{r}$ is a position vector contained within the interface and measured from the crack tip: if the diffraction vector (i.e. reciprocal vector defining orientation and spacing of lattice planes) in both crystallites is $\underset{\sim}{g}$ the fringes are loci of

$$\underset{\sim}{g} \cdot \underset{\sim}{c} = N \qquad (1)$$

where N is the order of the fringe [12]. Thus one characteristic of the displacement fringe system is that the observed pattern should remain geometrically similar for all reflections. In Figs. 6 and 8, where the effects of systematically varying $\underset{\sim}{g}$ are investigated, the geometry of the fringe pattern is seen to change markedly. Moreover, the reflections in Fig. 8 are such that we would have $\underset{\sim}{g} \cdot \underset{\sim}{c} \approx 0$ if the mutual crack-wall displacements were, as anticipated, to be closely normal to the plane of the interface (hence of the foil). We must generally conclude that the displacement fringe system can be of no more than secondary importance in the micrographs observed in this work.

The moiré fringe system, on the other hand, is generated when the overlapping crystal portions have a small mismatch in lattice periodicity such that there is a small difference in diffraction vector, $\delta\underset{\sim}{g} = \underset{\sim}{g}_1 - \underset{\sim}{g}_2 \neq 0$. The fringes are then loci of [13, 14]

$$\delta\underset{\sim}{g} \cdot \underset{\sim}{r} = \text{const.} \qquad (2)$$

Then since $\delta\underset{\sim}{g}$ will generally vary with $\underset{\sim}{g}$, we would expect such a pattern to be reflection dependent, consistent with the observations of Figs. 6 and 8. This diagnosis in favour of the moiré system was also reached in the earlier X-ray analysis of remnant cone cracks in silicon [5]. In the event that the opposing crack walls are able to recontact and heal, interfacial relaxation of the mismatched crystal portions results in a dislocation network [8, 15]. Examples of spontaneous crack healing are seen in Figs. 7 (near-tip region) and 9.

It is of interest to determine the degree of mismatch needed to explain the network patterns seen in the micrographs. Characterising the fringe system associated with the non-healed crack interfaces by the moiré vector (i.e. reciprocal vector defining orientation and spacing of fringe system) [13]

$$\underset{\sim}{G} = \delta\underset{\sim}{g} = \underset{\sim}{g}_1 - \underset{\sim}{g}_2, \tag{3}$$

we distinguish between two basic moiré configurations: <u>parallel</u> moirés, in which $\underset{\sim}{g}_1$ and $\underset{\sim}{g}_2$ differ slightly in magnitude ($\underset{\sim}{G}$ parallel to $\underset{\sim}{g}$), and <u>rotation</u> moirés, in which $\underset{\sim}{g}_1$ and $\underset{\sim}{g}_2$ differ slightly in direction ($\underset{\sim}{G}$ perpendicular to $\underset{\sim}{g}$). In most cases examined here the system appeared to be predominantly of the second type; note in particular the comparative absence of fringe contrast in Fig. 8c, corresponding to $\underset{\sim}{G}$ having a large component parallel to $\underset{\sim}{g}$. Such a lattice-plane rotation is in fact consistent with a simple shear displacement field $\underset{\sim}{u} = u_z(r)\underset{\sim}{\hat{z}}$ ($\underset{\sim}{\hat{z}}$ being a unit vector parallel to the crack front) for the crack walls at the interface (i.e. "mode III" field). Writing $d = \left|\underset{\sim}{g}\right|^{-1}$ as the spacing of the lattice planes and $D = \left|\underset{\sim}{G}\right|^{-1}$ as the spacing of the moiré fringes, we obtain

$$\frac{D}{d} \approx \frac{1}{\varepsilon} \qquad \text{(rotation)} \tag{4}$$

with ε the angular misorientation of the diffracting planes. Typically, we have $d_{11\bar{2}0} \approx 0.15$ nm (α-SiC), $D \approx 0.1$ μm (Fig. 8), from which we compute a "lattice mismatch" $d/D \approx 1 \times 10^{-3}$; this corresponds to a mutual lattice-plane misorientation $\varepsilon \approx u_z(r)/r \approx 1 \times 10^{-3}$ rad.

Our treatment here is necessarily oversimplistic: a more accurate account of fringe pattern details would require a rigorous diffraction contrast analysis, taking into account such complications as inclinations of the interface to the foil surface [14], superposition of components $u_y(r)\hat{\underset{\sim}{y}}$ and $u_x(r)\hat{\underset{\sim}{x}}$ ($\hat{\underset{\sim}{y}}$ and $\hat{\underset{\sim}{x}}$ being unit vectors parallel to crack normal and crack direction respectively) onto the residual displacement field (i.e. adding "modes I and II" to "mode III"), etc., in the general reflection situation.

3.3 Other interfacial features in the crack images

Some other contrast features were evident at the residual crack interfaces. The crack front itself usually showed up by enhanced diffraction contrast, implying residual crack-tip strain due to incomplete closure of the interface. This residual-strain effect was more evident in some cases (e.g. Fig. 8) than others (e.g. Fig. 7); in general, those interfaces indicating some tendency to healing showed the least crack-tip contrast. In addition, the contrast visibility increased in intensity from zero as the $\underset{\sim}{g}$ vector was rotated away from alignment with the crack front, in accordance with a state of plane strain at the tip: a particularly clear example of this contrast variation is shown in Fig. 10.

The existence of a residual crack opening points to the operation of some closure-prevention mechanism. While there was ample indication of dislocation generation about the central, grossly deformed regions of the indentations, in no case was there found any evidence for dislocation activity in association with crack growth, thus ruling out plastic flow as a significant factor.* The present observations merely reinforce similar conclusions previously drawn concerning the reversibility of fracture in highly brittle solids [5, 8, 15]. Closure resistance may be identified with purely mechanical obstruction, predominantly from cleavage steps at the fracture surfaces [5]. These are seen clearly in many of the micrographs, notably in Figs. 8 and 9. A close study of the mechanics of formation of such steps [16] indicates a process in which crack segments propagating on closely adjacent planes first overlap and subsequently link up tip-to-plane to effect separation. Segmentation of an initially planar crack into an array of partial fronts occurs when a "twist-mode" disturbance is suddenly encountered in the crack propagation field [17]. Fig. 11 depicts the phenomenon schematically, and illustrates via the fringe pattern in the accompanying micrograph the significant influence the stepped regions have on the residual crack opening. The

---

*The healing dislocations do not, of course, form via a glide process, but rather as a direct consequence of crack closure; they could therefore hardly contribute to a residual crack opening.

smallest of lateral displacements across the crack interface, corresponding to the lattice mismatch of order one part in a thousand typified by the fringe spacings, could be quite sufficient to prevent the opposing walls from keying together in perfect registry upon removal of the indenter load. Moreover, these same lateral displacements would account for a predominance of a mode III type configuration in the moire system.

One further detail which was observed in isolated cases was the trace of a slightly retracted crack front. This is especially noticeable in Fig. 10, where protuberant cleavage-step damage beyond the residual interfacial opening gives some indication as to how far the crack front must once have extended. The exact source of this detail is not clear, but its contrast parallels that of dislocations and thus probably arises from residual displacements on the atomic scale.

3.4 Cracks subjected to special treatments

Some of the indented sapphire specimens were subjected to a mechanical shock treatment prior to thinning. This was done simply by delivering a small impulse, insufficient to rupture the specimen, to the surface opposite to that containing the indentations. The chief result of this treatment was to re-propagate the existing median vent cracks (the lateral vents suffering effectively zero tension in the flexural impulse), to anything up to an order of magnitude increase in length, rather than to change the nature of the patterns. These extended crack portions also showed some tendency to partial spontaneous healing [8].

Other specimens were given an anneal treatment. In this case diffusion and sintering processes led to a marked enhancement in the healing [8]. Fig. 12 shows a remnant interface at which the delineation between restored and non-restored interfacial regions is distinct. Elongated "pipes" are seen to form along lines of greatest residual mismatch, namely along network dislocations, but these tend ultimately to break up into small polyhedral voids in the regions of more prolonged sintering away from the open interface.

4. Discussion

The observations described here provide useful semi-quantitative information on the geometry of residual cracks about micro-indentations. It should be emphasised, however, that this information relates only to the history of the propagation, and not the initiation, of the cracks. That is to say, nothing in the electron micrographs revealed any indication as to how the cracks originally nucleated and formed. It is known from earlier section-and-etch examinations [3] that both median- and lateral-vent initiation is tied up intimately with events within the gross deformation zone immediately surrounding the indenter; unfortunately, this is the region of lost resolution and diffraction-pattern blurring (Sect. 3.1), and, while it is clear that the theoretical strength limits of the lattice are undoubtedly approached (at least in the most brittle of solids), the nature of indentation-induced deformation remains obscure [9, 10, 18, 19]. This is one aspect of the indentation problem which calls for a good deal more attention.

Although we have given explicit attention here to only sapphire and α-silicon carbide, the crack patterns described appear to be quite typical of highly brittle solids in general. In particular, the vent-crack systems show the same broad geometrical features evident in such structurally diverse materials as monocrystalline silicon and amorphous silicates [3, 20], thus emphasising the dominant role of the indentation stress field in determining the fracture paths. Nevertheless, preferred cleavage tendencies do usually have some effect on indentation-cracking geometry [4, 21], and crystallographic tendencies were indeed noted in the present observations. In this respect the materials studied in the present work provide an interesting contrast in that α-silicon carbide has a distinct tendency to basal cleavage while sapphire does not, the reason being that although (0001) may represent the plane intersecting the least number of bonds in the hexagonal structure a relatively large component of polarity in the bonding in the case of sapphire renders this plane unfavourable on the grounds of electrostatic attraction effects [22]. One would therefore anticipate a greater incidence of lateral venting nearly parallel to (0001) foils in the former material; this trend was in fact apparent in the micrographs (note extensive crack plane in Figs. 8 and 10, not generally seen in sapphire). This raises the question of anisotropy in the microfracture, a factor which has already been recognised as one of vital importance in the interpretation of deformation processes in hardness testing [23]. One striking manifestation of anisotropy in a (cumulative) indentation chipping process occurs in the abrasion of diamond; by changing

the abrasion direction on a given surface the wear rate may alter by as much as three orders of magnitude [24]. Anisotropy is therefore a second topic which warrants further consideration in relation to indentation fracture.

The present results also bear on the process of crack healing, and on the agencies which tend to obstruct it. In those special instances where spontaneous healing was observed, evidence of cleavage steps and "debris" at the interface was conspicuously absent [15]. (It is possible, of course, that the very act of thinning the foil removes, at least partially, some of these obstructions.) Here again the two materials examined showed contrasting behaviour, for the only sighting of a spontaneously healed area in silicon carbide was that shown in Fig. 10. The nature of the bonding thus appears to manifest itself in the mechanics of the closure as well as of the opening of the cracks; the explanation is once more to be sought in the long-range electrostatic attractive forces that tend to develop across fracture interfaces in ionic structures [25, 26]. The second type of healing reported here, that arising from mass transport at elevated temperatures, occurs in both materials. On the other hand, while indentation-induced cracks can be made to heal, so can they be made to extend still further, as in the event of mechanical shock. The existence of residual cracks of this sort has obvious implications in the strength of structural ceramics: an incompletely restored lattice across any separation interface represents a potential source of weakness in the material. A more detailed investigation into electron microscopic

images of fracture interfaces is accordingly under way, and will be reported at a later date [27]. For the present, it is sufficient to point out that the strengths of brittle materials can be seriously degraded by the most minute of contact events, and that this degradation may vary according to subsequent mechanical and thermal history.

Acknowledgements

The authors are indebted to S. M. Wiederhorn and M. V. Swain for valuable discussions on the work. They also acknowledge the sponsorship by the Office of Naval Research under Contract No. NR-032-535.

References

1. "The Science of Hardness Testing and its Research Applications," Symposium Proceedings, Eds. J. H. Westbrook and H. Conrad (American Society for Metals, 1973).

2. A. Kelly, "Strong Solids" (Clarendon, Oxford, 1966), Ch. 1.

3. B. R. Lawn and M. V. Swain, J. Mater. Sci. (in press).

4. B. R. Lawn and T. R. Wilshaw, J. Mater. Sci. (in press).

5. J. S. Williams, B. R. Lawn and M. V. Swain, Phys. Stat. Sol. (a) 2 (1970) 7.

6. B. J. Hockey, Ref. [1], Ch. 3.

7. B. J. Hockey, J. Amer. Ceram. Soc. 54 (1971) 223.

8. S. M. Wiederhorn, B. J. Hockey and D. E. Roberts, Phil. Mag. 28 (1973) 783.

9. V. G. Eremenko and V. I. Nikitenko, Phys. Stat. Sol. (a) 14 (1972) 317.

10. M. J. Hill and D. J. Rowcliffe, J. Mater. Sci. 9 (1974) 1569.

11. P. B. Hirsch, A. Howie, R. B. Nicholson, D. W. Pashley and M. J. Whelan, "Electron Microscopy of Thin Crystals" (Plenum, New York, 1965).

12. U. Bonse, M. Hart and G. H. Schwuttke, Phys. Stat. Sol. 33 (1969) 361.

13. R. Gevers, Phil. Mag. 7 (1962) 1681

14. R. Gevers, J. van Landuyt and S. Amelinckx, Phys. Stat. Sol. 18 (1966) 325.

15. B. R. Lawn and T. R. Wilshaw, "Fracture of Brittle Solids" (Cambridge University Press, Cambridge, 1975), Ch. 2.

16. M. V. Swain, B. R. Lawn and S. J. Burns, J. Mater. Sci. 9 (1974) 175.

17. E. Sommer, Eng. Fract. Mech. 1 (1969) 539.

18. I. V. Gridneva, Yu V. Milman and V. I. Trefilov, Phys. Stat. Sol. (a) 14 (1972) 177.

19. F. M. Ernsberger, Ann. Rev. Mat. Sci. 2 (1972) 529.

20. D. J. Rowcliffe, unpublished work.

21. B. R. Lawn, J. Appl. Phys. 39 (1968) 4828.

22. G. A. Wolff and J. D. Broder, Acta Cryst. 12 (1959) 313.

23. C. A. Brookes, J. B. O'Neill and B. A. W. Redfern, Proc. Roy. Soc. Lond. A322 (1971) 73.

24. E. M. Wilks and J. Wilks, Phil. Mag. 4 (1959) 158.

25. P. J. Bryant, L. H. Taylor and P. L. Gutshall, Trans. Tenth National Vacuum Sympos. (Macmillan, New York, 1963), p. 21.

26. J. A. Ryan and J. J. Grossman, Science J. 4 (1968) 41.

27. B. J. Hockey, to be published.

Figure Captions

1. Transmission electron micrograph showing typical configuration of dislocations and cracks associated with a room temperature 200 g Vickers indentation on the (0001) plane of α-SiC (4H polytype structure). Two distinct crack configurations are evident: A, radially directed cracks extending from corners of pyramidal impression, and B, cracks lying parallel to foil either partially or fully encircling central deformation zone (see also Figs. 8 and 10).

2. Transmission electron micrograph showing room temperature 200 g Knoop indentation on the $(10\bar{1}0)$ plane of Al_2O_3. Note crack remnants extending from sides of central deformation zone. Geometry of cracks depicted in Fig. 5.

3. Schematic presentation of median vent cracks, formed during indenter loading. Cracks are indicated by full, heavy lines, central deformation zone by dark region. (a) Section view, for both Vickers and Knoop indenters; location of eventual thin foil indicated by dashed lines. (b) Plan view, for Vickers indenter; crack tends to extend well beyond central zone, along both diagonals. (c) Plan view, for Knoop indenter; crack tends to be obscured below central zone, and to grow only along major diagonal.

4. Schematic representation of lateral vent cracks, formed during indenter unloading. Cracks are indicated by full, heavy lines (preceding median vent cracks by full, light lines), central deformation zone indicated by dark region. (a) Section view, for both Vickers and Knoop indenters; location of eventual thin foil indicated by dashed lines. (b) Plan

view, for Vickers indenter. (c) Plan view, for Knoop indenter. Note lateral vents tend to form as lobes between the median vents.

5. Effect of skew loading on crack pattern for Knoop indenter. Depicted to match loading conditions for the indentation illustrated in Fig. 2. (a) Section view. (b) Plan view.

6. Median vent type crack associated with 200 g Vickers indentation on (0001) plane of α-SiC, seen under different diffracting conditions. Crack front indicated as CC. (a) and (b) satisfy Laue reflection conditions, diffraction vectors shown. (c) is view of crack obtained by tilting specimen, multiple reflections. Note change in mismatch fringe pattern in (a) and (b) with diffraction vector. Specimen indented at room temperature and annealed in air at 1200^{o}C for four hours prior to thinning.

7. Portion of median vent crack associated with room temperature 200 g Vickers indentation on (0001) plane of Al_2O_3. Note complex fringe pattern over greater part of crack interface, with interfacial dislocation network near crack front CC. Multiple reflections operating.

8. Enlargement of lateral vent segment B in Fig. 1, under different reflecting conditions. Note tendency for fringes to run nearly parallel to the crack front, with modification in patterns at steps, S, which terminate at crack front. Diffraction vectors indicated.

9. Enlargement of lateral vent at left in Fig. 2. Note interfacial dislocation network between steps, S, which terminate at crack front.

10. Enlargement of lateral vent segment B′ in Fig. 1, under different reflecting conditions. Note disappearance of crack-tip contrast

for $\underset{\sim}{g}$ parallel to front. Note also presence of features exhibiting dislocation-like contrast ahead of residual crack front. Step contrast, S, indicates extent to which crack front must once have propagated.

11. (a) Portion of remnant crack front associated with room temperature 200 g Vickers indentation on (0001) α-SiC.

(b) Schematic representation, showing how crack breaks up into partial fronts upon encountering some shear disturbance.

Arrows indicate direction of propagation of main crack.

12. Median vent crack remnant associated with room temperature 200 g Vickers indentation on (0001) Al_2O_3. Indented specimen annealed at 1200°C in air for 8 hr prior to thinning. Annealing results in recession of crack front to C′C′, with healed (sintered) region characterised by interfacial dislocations and voids, and unhealed (open) region characterised by mismatch fringe contrast.


A
B
A
B
A
A
2 µm

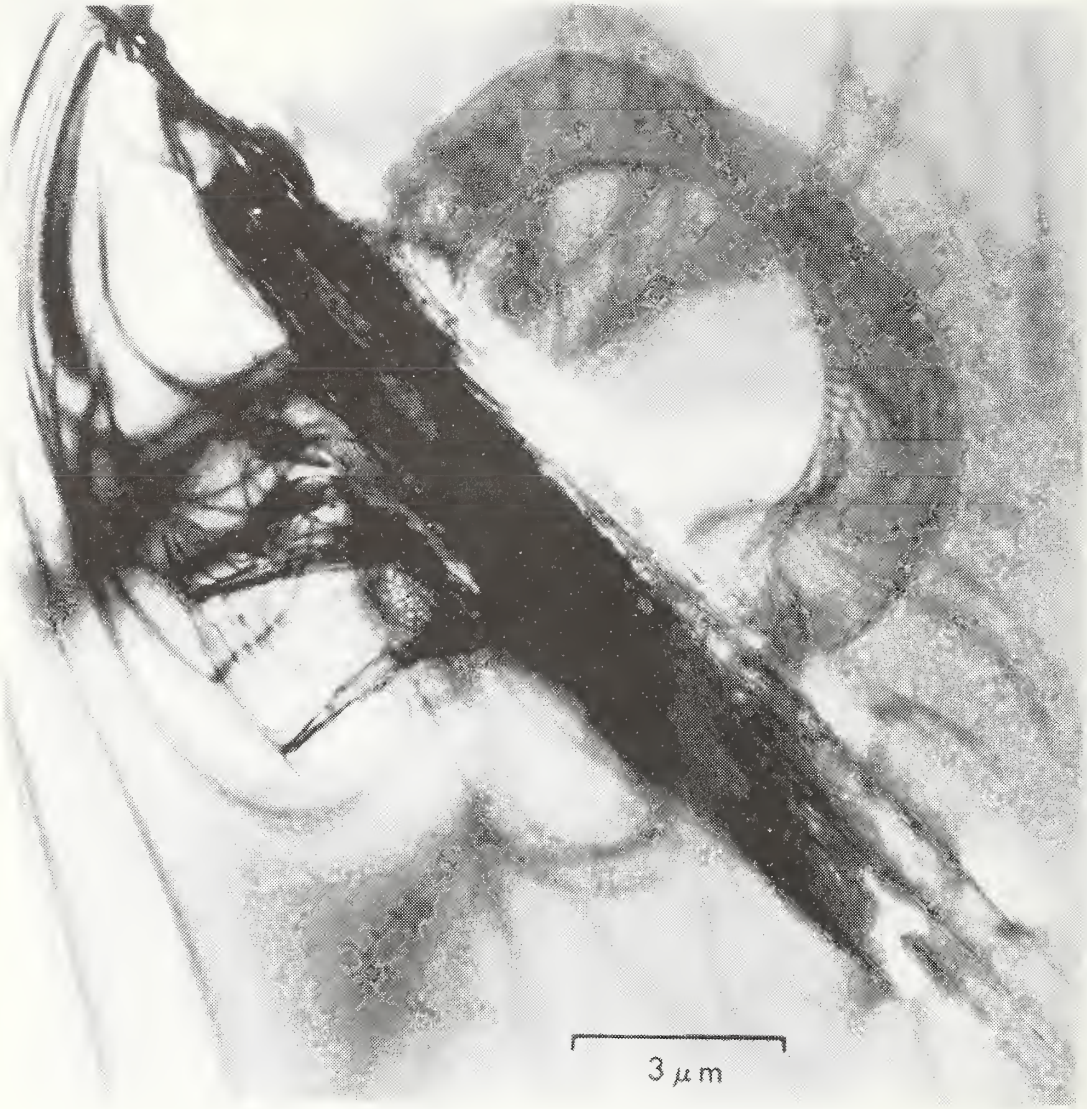

2.

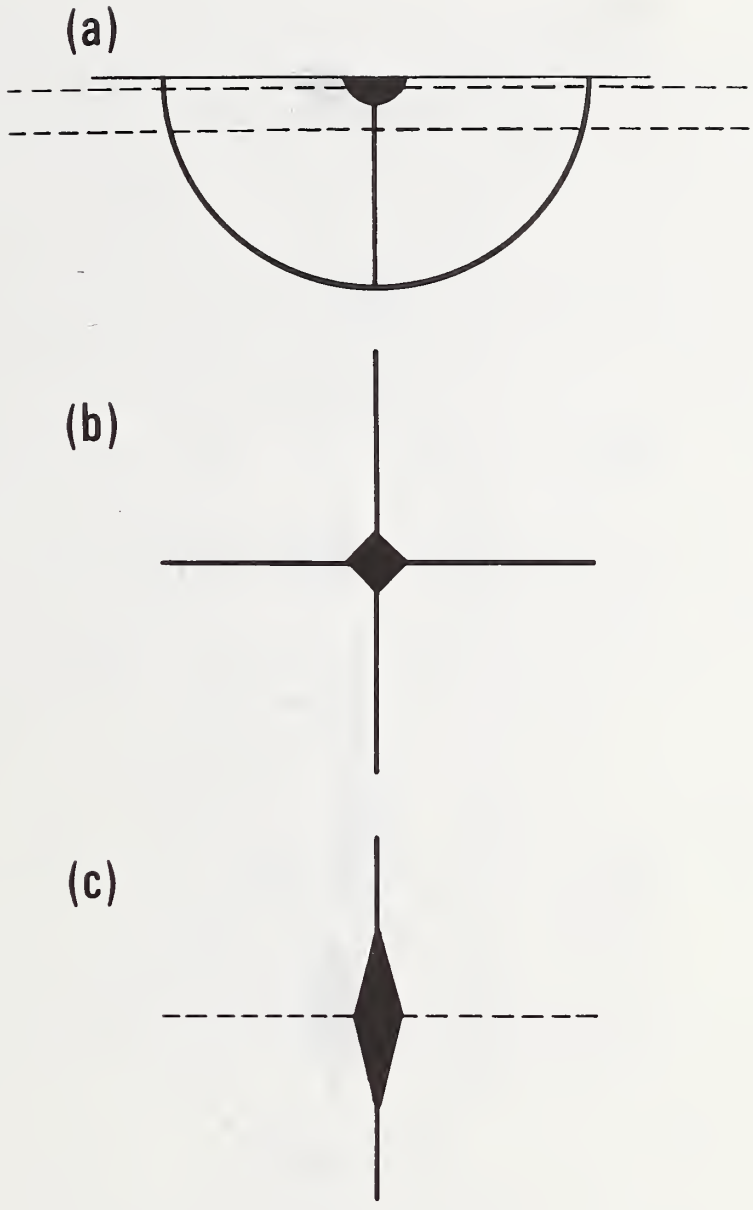
(a)
(b)
(c)

(a)

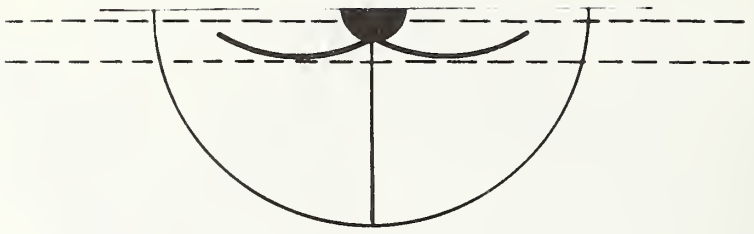

(b)

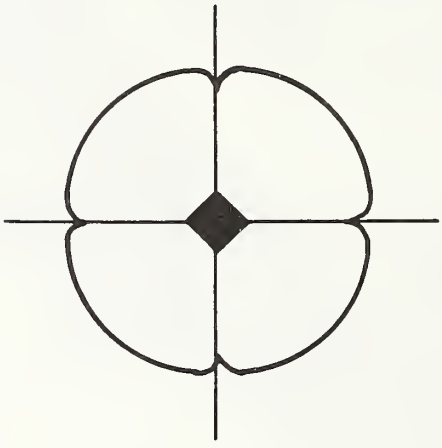

(c)

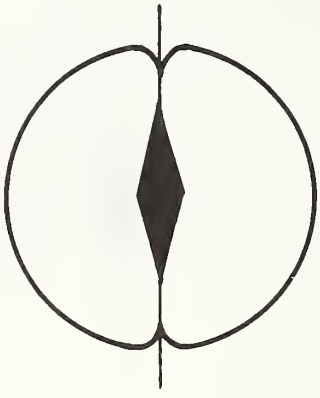

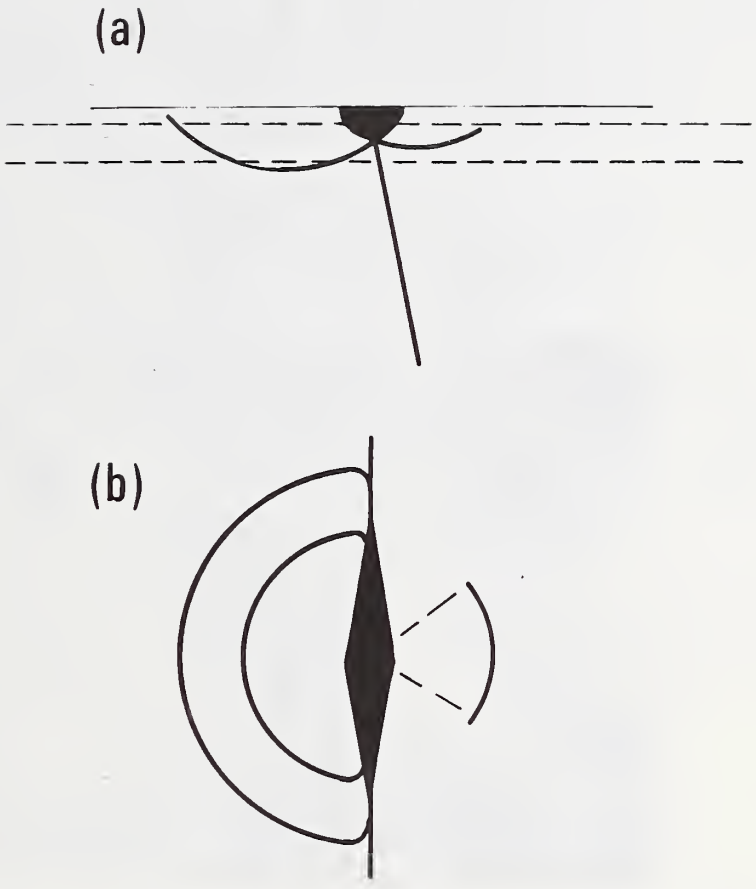
(a)
(b)

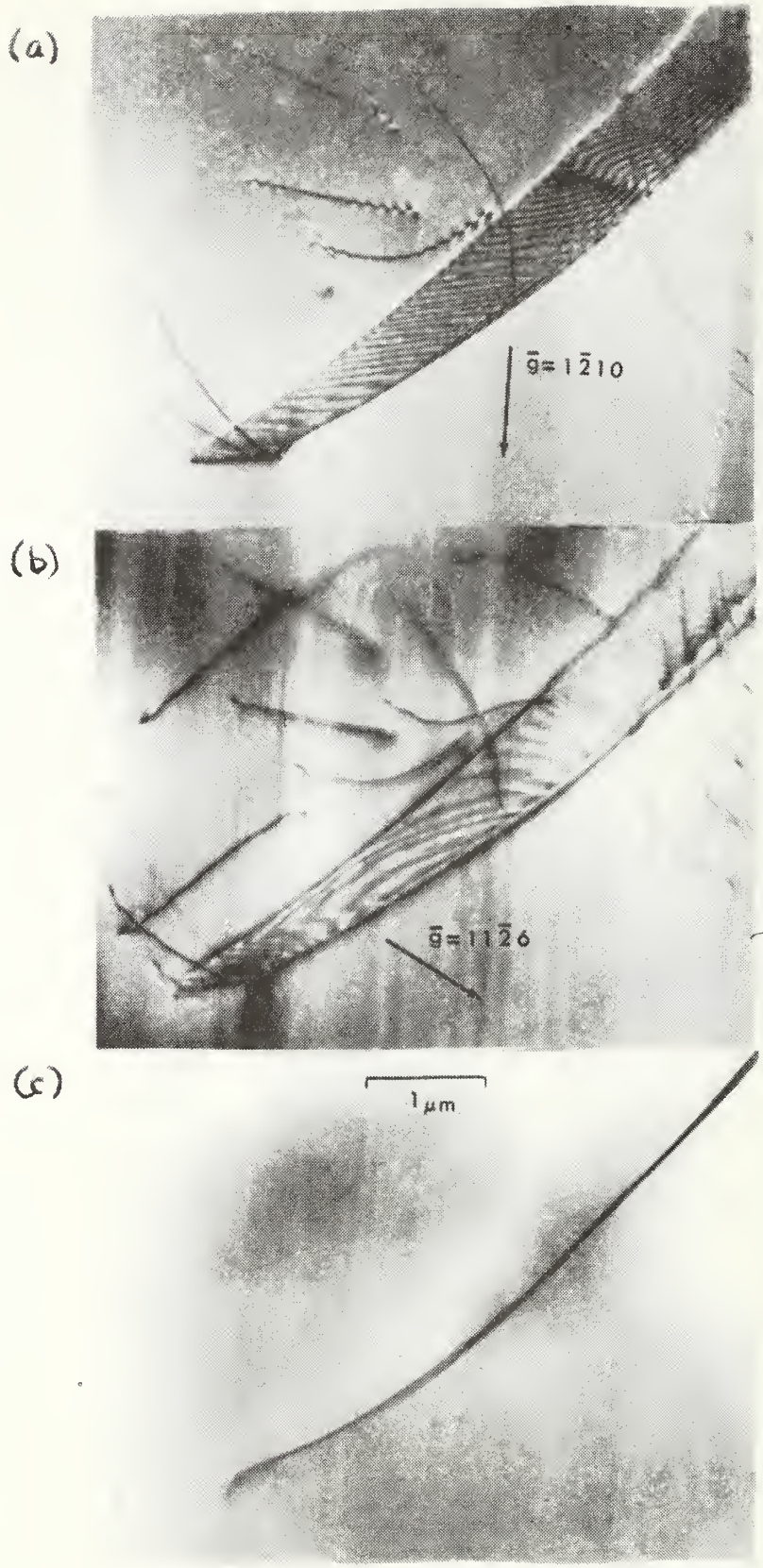
(a)
$\vec{g}=1\bar{2}10$
(b)
$\vec{g}=11\bar{2}6$
(c)
1 μm

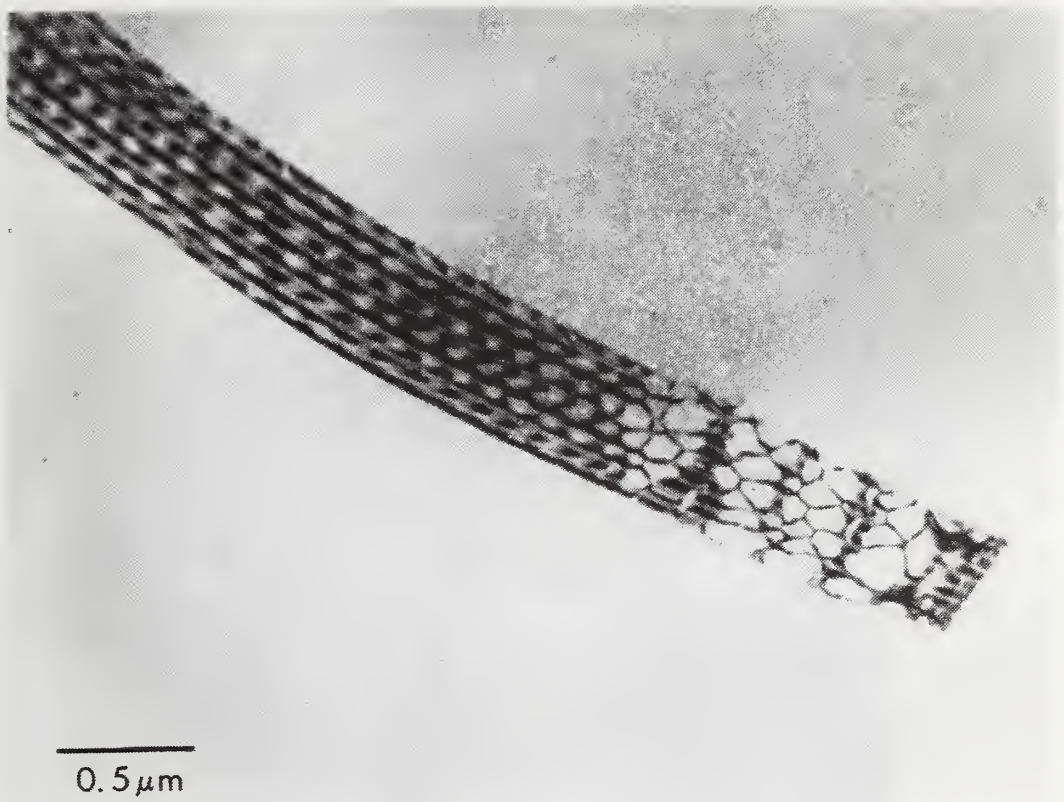
0.5 μm

(a)

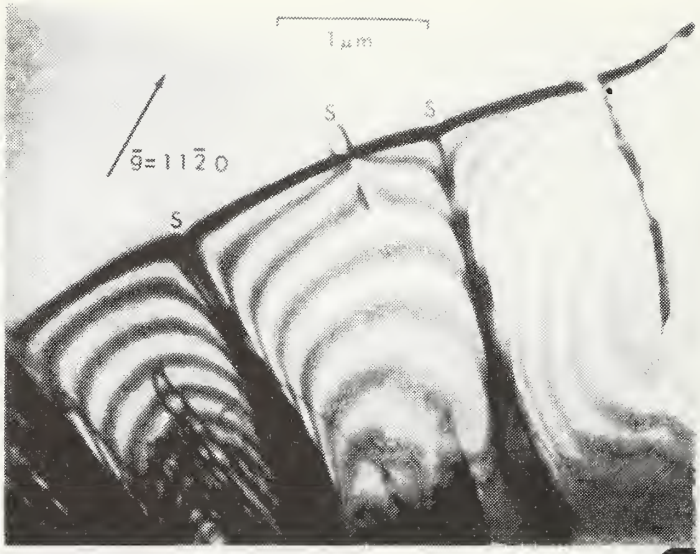
1 μm
$\vec{g}=11\bar{2}0$
S
S
S

(b)

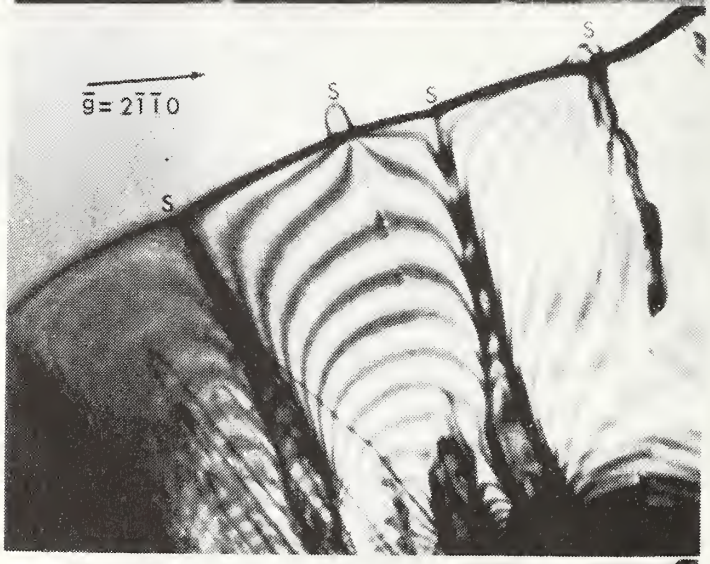
$\vec{g}=2\bar{1}\bar{1}0$
S
S
S
S

(c)

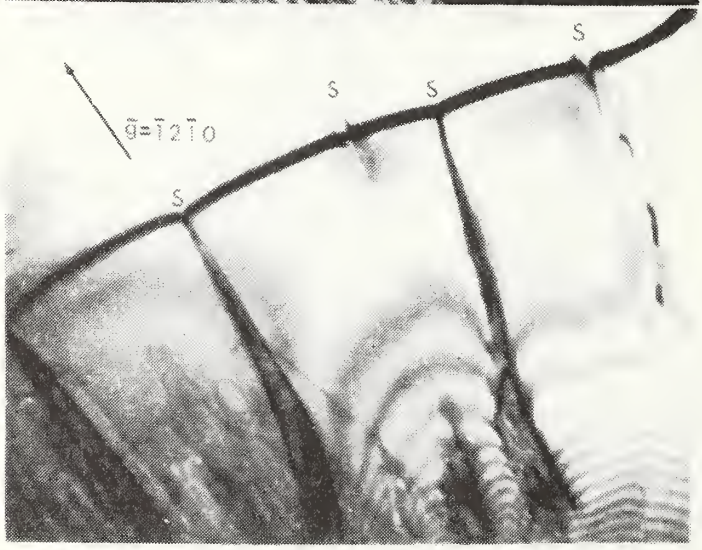
$\vec{g}=\bar{1}2\bar{1}0$
S
S
S
S

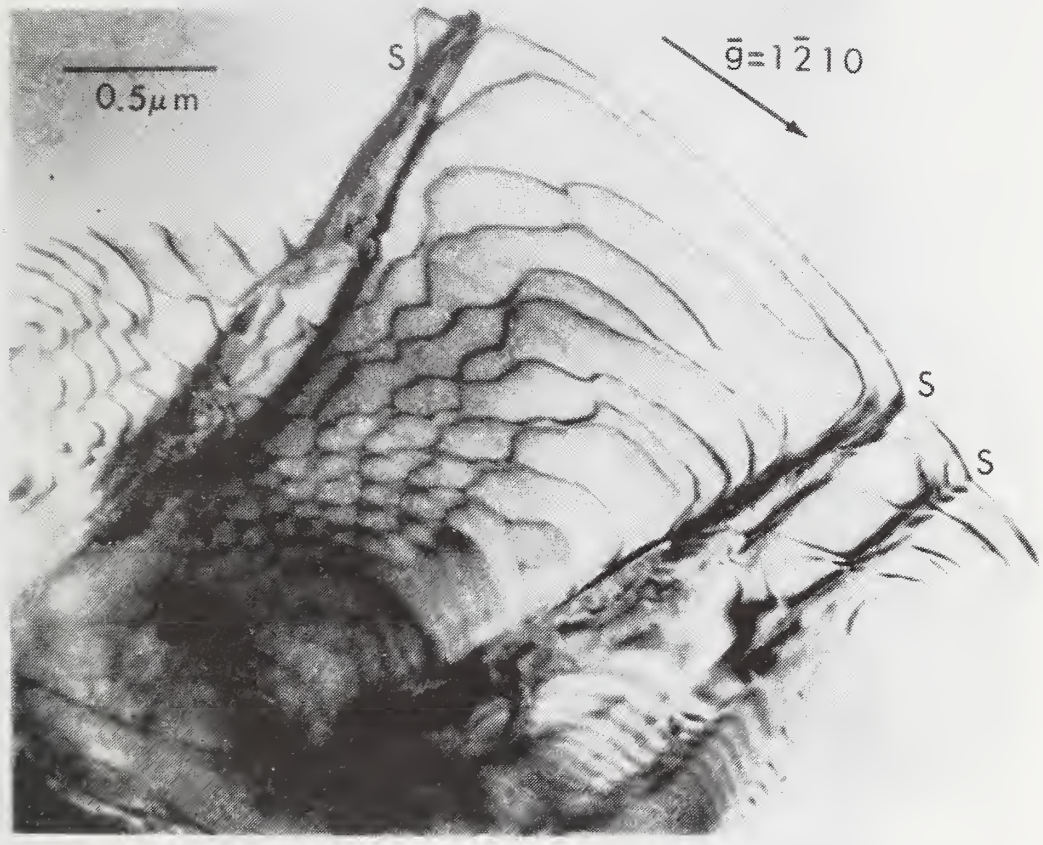
0.5μm
S
$\bar{g}=1\bar{2}10$
S
S

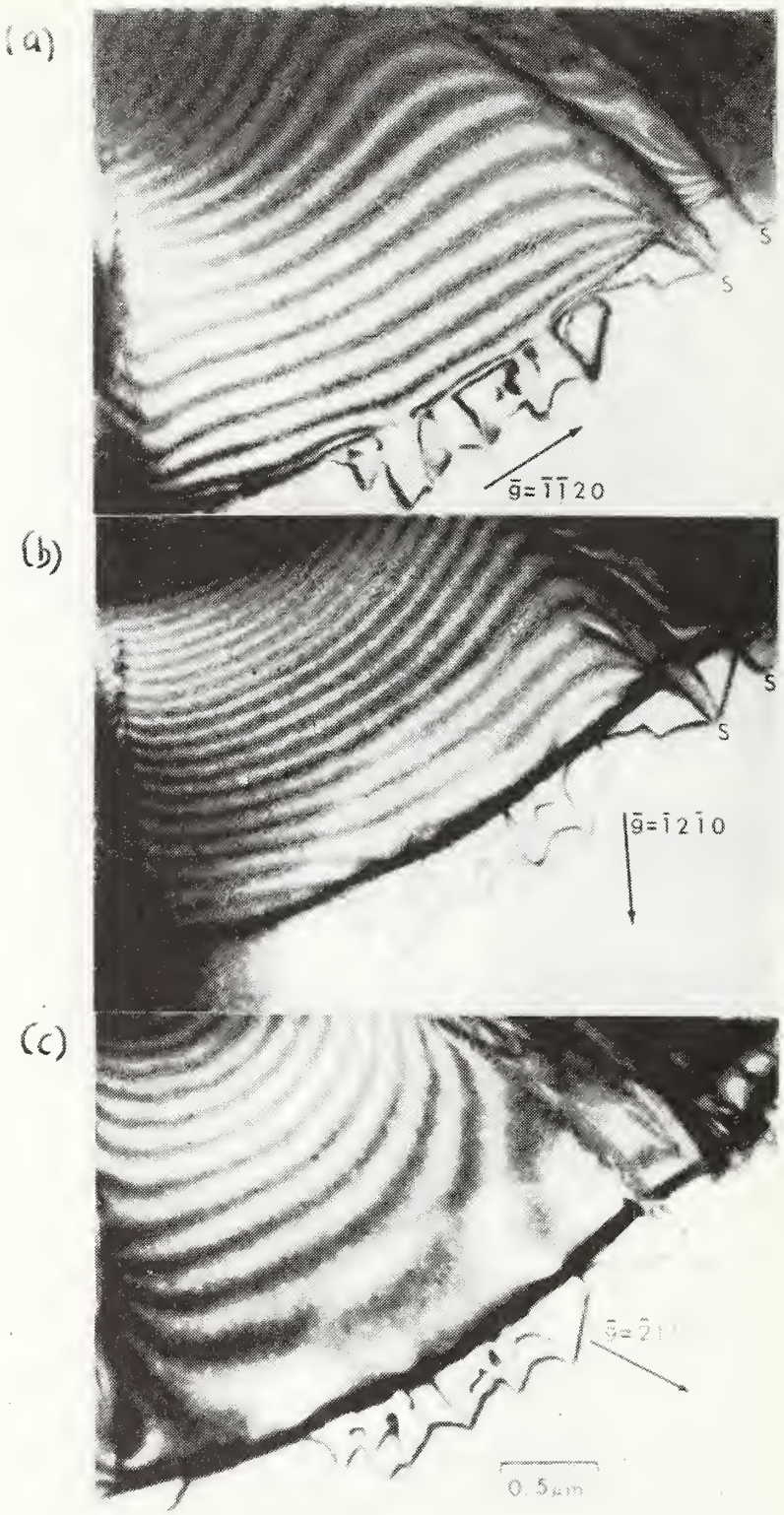
(a)
S
S
$\bar{g}=\bar{1}\bar{1}20$
(b)
S
S
$\bar{g}=\bar{1}2\bar{1}0$
(c)
0.5 μm

(a)

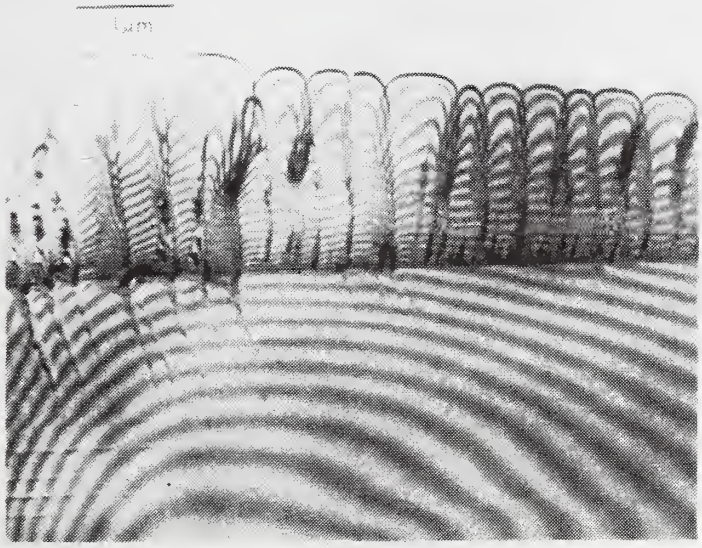

(b)

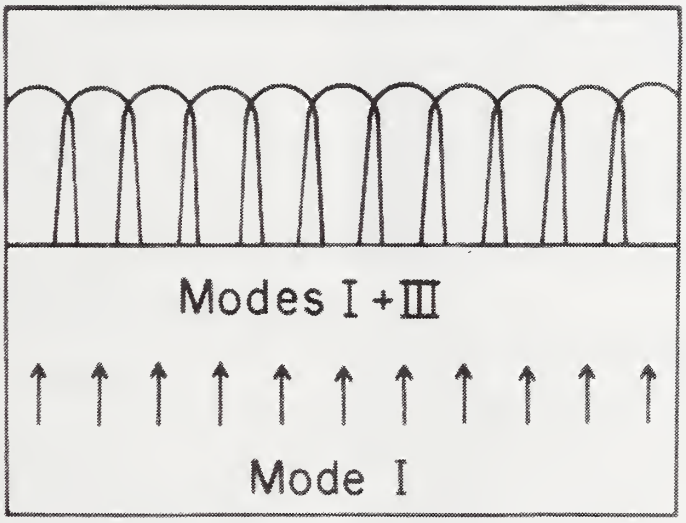

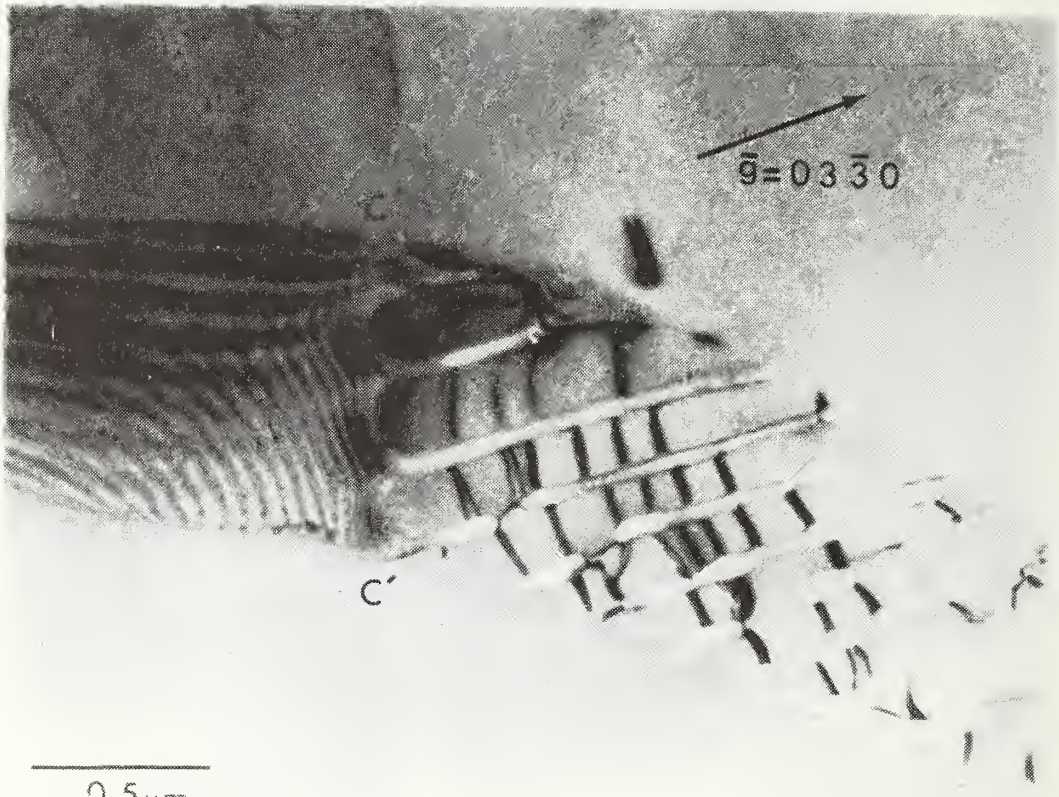

0.5μm

DISTRIBUTION LIST

Organization

Office of Naval Research
Department of the Navy
Attn: Code 471
Arlington, Virginia 22217

Director
Office of Naval Research
Branch Office
495 Summer Street
Boston, Massachusetts 02210

Director
Office of Naval Research
New York Area Office
207 West 24th Street
New York, New York 10011

Director
Office of Naval Research
Branch Office
1030 East Green Street
Pasadena, California 91101

Commanding Officer
Naval Weapons Laboratory
Attn: Research Division
Dahlgren, Virginia 22448

Director
Naval Research Laboratory
Attn: Technical Information Officer
Code 2000
Washington, D. C. 20390

Director
Naval Research Laboratory
Attn: Technical Information Officer
Code 2020
Washington, D. C. 20390

Director
Naval Research Laboratory
Attn: Technical Information Officer
Code 6000
Washington, D. C. 20390

Organization

Director
Naval Research Laboratory
Attn: Technical Information Officer
Code 6100
Washington, D. C. 20390

Director
Naval Research Laboratory
Attn: Technical Information Officer
Code 6300
Washington, D. C. 20390

Director
Naval Research Laboratory
Attn: Technical Information Officer
Code 6400
Washington, D. C. 20390

Director
Naval Research Laboratory
Attn: Library
Code 2029 (ONRL)
Washington, D. C. 20390

Commander
Naval Air Systems Command
Department of the Navy
Attn: Code AIR 320A
Washington, D. C. 20360

Commander
Naval Air System Command
Department of the Navy
Attn: Code AIR 5203
Washington, D. C. 20360

Commander
Naval Ordnance Systems Command
Department of the Navy
Attn: Code ORD 033
Washington, D. C. 20360

Commanding Officer
Naval Air Development Center
Aeronautical Materials Div.
Johnsville
Attn: Code MAM
Warminster, Pa. 18974

Commanding Officer
Naval Ordnance Laboratory
Attn: Code 210
White Oak
Silver Spring, Maryland 20910

Commander
Naval Ship Systems Command
Department of the Navy
Attn: Code 0342
Washington, D. C. 20360

Commanding Officer
Naval Civil Engineering Laboratory
Attn: Code L70
Port Hueneme, California 93041

Commander
Naval Ship Engineering Center
Department of the Navy
Attn: Code 6101
Washington, D. C. 20360

Naval Ships R&D Laboratory
Annapolis Division
Attn: Code A800
Annapolis, Maryland 21402

Commanding Officer
Naval Ships R&D Center
Attn: Code 747
Washington, D. C. 20007

Commander Naval Weapons Center
Naval Weapons Center
Attn: Code 5560
China Lake, California 93555

Commander
Naval Underseas Warfare Center
Pasadena, California 92152

Scientific Advisor
Commandant of the Marine Corps
Attn: Code AX
Washington, D. C. 20380

Commanding Officer
Army Research Office, Durham
Box CM, Duke Station
Attn: Metallurgy & Ceramics Div.
Durham, North Carolina 27706

Office of Scientific Research
Department of the Air Force
Attn: Solid State Div. (SRPS)
Washington, D. C. 20333

Defense Documentation Center
Cameron Station
Alexandria, Virginia 22314

National Bureau of Standards
Attn: Metallurgy Division
Washington, D. C. 20234

National Bureau of Standards
Attn: Inorganic Materials Div.
Washington, D. C. 20234

Atomic Energy Commission
Attn: Metals & Materials Branch
Washington, D. C. 20545

Argonne National Laboratory
Metallurgy Division
P. O. Box 299
Lemont, Illinois 60439

Brookhaven National Laboratory
Technical Information Division
Attn: Research Library
Upton, Long Island, New York 11973

Library
Bldg. 50, Room 134
Lawrence Radiation Laboratory
Berkeley, California 94720

Los Alamos Scientific Laboratory
P. O. Box 1663
Attn: Report Librarian
Los Alamos, New Mexico 87544

Commanding Officer
Army Materials and Mechanics
Research Center
Attn: Res. Programs Office (AMXMR-P)
Watertown, Massachusetts 02172

Director
Metals & Ceramics Division
Oak Ridge National Laboratory
P. O. Box X
Oak Ridge, Tennessee 37830

Commanding Officer
Naval Underwater Systems Center
Newport, Rhode Island 02844

Aerospace Research Laboratories
Wright-Patterson AFB
Building 450
Dayton, Ohio 45433

Defense Metals Information Center
Battelle Memorial Institute
505 King Avenue
Columbus, Ohio 43201

Army Electronics Command
Evans Signal Laboratory
Solid State Devices Branch
c/o Senior Navy Liaison Officer
Fort Monmouth, New Jersey 07703

Commanding General
Department of the Army
Frankford Arsenal
Attn: ORDBA-1320, 64-4
Philadelphia, Pennsylvania 19137

Executive Director
Materials Advisory Board
National Academy of Sciences
2101 Constitution Avenue, N. W.
Washington, D. C. 20418

NASA Headquarters
Attn: Code RRM
Washington, D. C. 20546

Air Force Materials Lab
Wright-Patterson AFB
Attn: MAMC
Dayton, Ohio 45433

Air Force Materials Lab
Wright-Patterson AFB
Attn: MAAM
Dayton, Ohio 45433

Deep Submergence Systems Project
Attn: DSSP-00111
Washington, D. C. 20360

Advanced Research Projects Agency
Attn: Director, Materials Science
Washington, D. C. 20301

Department of the Interior
Bureau of Mines
Attn: Science & Engineering Advisor
Washington, D. C. 20240

Defense Ceramics Information Center
Battelle Memorial Institute
505 King Avenue
Columbus, Ohio 43201

National Aeronautics & Space Adm.
Lewis Research Center
Attn: Librarian
21000 Brookpark Rd.
Cleveland, Ohio 44135

Naval Missile Center
Materials Consultant
Code 3312-1
Point Mugu, California 93041

Commanding Officer
Naval Weapons Center Corona Labs.
Corona, California 91720

Commander
Naval Air Test Center
Weapons Systems Test Div. (Code 01A)
Patuxent River, Maryland 20670

Director
Ordnance Research Laboratory
P. O. Box 30
State College, Pennsylvania 16801

Director
Applied Physics Laboratory
1013 Northeast Fortieth St.
Seattle, Washington 98105

Materials Sciences Group
Code S130.1
271 Catalina Boulevard
Navy Electronics Laboratory
San Diego, California 92152

Dr. Waldo K. Lyon
Director, Arctic Submarine Laboratory
Code 90, Building 371
Naval Undersea R&D Center
San Diego, California 92132

Dr. R. Nathan Katz
Ceramics Division
U.S. Army Materials & Mechanics
Research Center
Watertown, Mass. 02172

SUPPLEMENTARY DISTRIBUTION LIST

Professor R. Roy
Materials Research Laboratory
Pennsylvania State University
University Park, Pennsylvania 16802

Professor D. H. Whitmore
Department of Metallurgy
Northwestern University
Evanston, Illinois 60201

Professor J. A. Pask
Department of Mineral Technology
University of California
Berkeley, California 94720

Professor D. Turnbull
Div. of Engineering and Applied Sci.
Harvard University
Pierce Hall
Cambridge, Massachusetts 02100

Dr. T. Vasilos
AVCO Corporation
Research and Advanced Development Div.
201 Lowell St.
Wilmington, Massachusetts 01887

Dr. H. A. Perry
Naval Ordnance Laboratory
Code 230
Silver Spring, Maryland 20910

Dr. Paul Smith
Crystals Branch, Code 6430
Naval Research Laboratory
Washington, D. C. 20390

Dr. A. R. C. Westwood
RIAS Division
Martin-Marietta Corporation
1450 South Rolling Road
Baltimore, Maryland 21227

Dr. W. Haller
Chief, Inorganic Glass Section
National Bureau of Standards
Washington, D. C. 20234

Dr. R. H. Doremus
General Electric Corporation
Metallurgy and Ceramics Lab.
Schenectady, New York 12301

Professor G. R. Miller
Department of Ceramic Engineering
University of Utah
Salt Lake City, Utah 84112

Dr. T. D. Chikalla
Fuels and Matls. Department
Battelle Northwest
P. O. Box 999
Richland, Washington 99352

Mr. I . Berman
Army Materials and Mechanics
Research Center
Watertown, Massachusetts 02171

Dr. F. F. Lange
Westinghouse Electric Corporation
Research Laboratories
Pittsburgh, Pennsylvania 15235

Professor H. A. McKinstry
Pennsylvania State University
Materials Research Laboratory
University Park, Pa. 16802

Professor T. A. Litovitz
Physics Department
Catholic University of America
Washington, D. C. 20017

Dr. R. J. Stokes
Honeywell Corporate Research Center
10701 Lyndale Avenue South
Bloomington, Minnesota 55420

Dr. Harold Liebowitz
Dean of Engineering
George Washington Univeristy
Washington, D. C. 20006

Dr. H. Kirchner
Ceramic Finishing Company
P. O. Box 498
State College, Pennsylvania 16801

Professor A. H. Heuer
Case Western Reserve University
University Circle
Cleveland, Ohio 44106

Dr. D. E. Niesz
Battelle Memorial Institute
505 King Avenue
Columbus, Ohio 43201

Dr. F. A. Kroger
University of Southern California
University Park
Los Angeles, California 90007

Dr. Sheldon M. Wiederhorn
National Bureau of Standards
Inorganic Materials Division
Washington, D. C. 20234

Dr. C. O. Hulse
United Aircraft Research Labs
United Aircraft Corporation
East Hartford, Connecticut 06108

Professor M. H. Manghnani
University of Hawaii
Hawaii Institute of Geophysics
2525 Correa Road
Honolulu, Hawaii 96822

Dr. Stephen Malkin
Department of Mechanical Engineering
University of Texas
Austin, Texas 78712

Prof. H. E. Wilhelm
Department of Mechanical Engineering
Colorado State University
Fort Collins, Colorado 80521

Stanford University
Dept. of Materials Sciences
Stanford, California 94305

Dr. R. K. MacCrone
Department of Materials Engineering
Rensselaer Polytechnic Institute
Troy, New York 12181

Dr. D. C. Mattis
Belfer Graduate School of Science
Yeshiva University
New York, New York 10033

Professor R. B. Williamson
College of Engineering
University of California
Berkeley, California 94720

Professor R.. W. Gould
Department of Metallurgical
and Materials Engineering
College of Engineering
University of Florida
Gainesville, Florida 32601

Professor V. S. Stubican
Department of Materials Science
Ceramic Science Section
Pennsylvania State University
University Park, Pennsylvania 16802

Dr. R. C. Anderson
General Electric Company
Miniature Lamp Department
Nela Park
Cleveland, Ohio 44112

Dr. Bert Zauderer
MHD Program, Advanced Studies
Room L-9513-VFSC
General Electric Company
P. O. Box 8555
Philadelphia, Pennsylvania 19101

Prof. C. F. Fisher, Jr.
Department of Mechanical and Aero-
Space Engineering
University of Tennessee
Knoxville, Tennessee 37916

USCOMM NBS DC

NBS-114A (REV. 7-73)

U.S. DEPT. OF COMM. BIBLIOGRAPHIC DATA SHEET	1. PUBLICATION OR REPORT NO. NBSIR 75-658	2. Gov't Accession No.	3. Recipient's Accession No.

4. TITLE AND SUBTITLE

Electron Microscopic Observations of Microcracking About Indentations in Aluminium Oxide and Silicon Carbide

5. Publication Date: January 1975

6. Performing Organization Code

7. AUTHOR(S)
B. J. Hockey and B. R. Lawn

8. Performing Organ. Report No.

9. PERFORMING ORGANIZATION NAME AND ADDRESS

NATIONAL BUREAU OF STANDARDS
DEPARTMENT OF COMMERCE
WASHINGTON, D.C. 20234

10. Project/Task/Work Unit No. 3130453

11. Contract/Grant No.

12. Sponsoring Organization Name and Complete Address *(Street, City, State, ZIP)*

Department of the Navy
Office of Naval Research
Arlington, Virginia 22217

13. Type of Report & Period Covered Interim 7/1/74---6/30/75

14. Sponsoring Agency Code ONR

15. SUPPLEMENTARY NOTES

16. ABSTRACT *(A 200-word or less factual summary of most significant information. If document includes a significant bibliography or literature survey, mention it here.)*

Transmission electron microscopy is used to examine the nature of microcracking about small-scale indentations in two highly brittle solids, sapphire and carborundum. The observed crack geometry is discussed in terms of an earlier model of indentation fracture beneath a point force, in which both loading and unloading half-cycles contribute to the crack growth. The residual interfaces are characterised mainly by moiré patterns, sometimes by dislocation networks. These observations are discussed in relation to spontaneous closure and healing mechanisms, and the "lattice mismatch" necessary for their production estimated at about one part in a thousand. It is shown that cleavage steps comprise the main source of obstruction to lattice restoration across the interfaces. Mechanical and thermal treatments of the indented surfaces are found to influence the extent of the residual cracking. Some practical implications of the observations are discussed.

17. KEY WORDS *(six to twelve entries; alphabetical order; capitalize only the first letter of the first key word unless a proper name; separated by semicolons)*

Brittle solids; dislocation networks; electron microscopy; healing; indentations; microcracking; moiré patterns

18. AVAILABILITY

☐ Unlimited

☒ For Official Distribution. Do Not Release to NTIS

☐ Order From Sup. of Doc., U.S. Government Printing Office Washington, D.C. 20402, SD Cat. No. C13

☐ Order From National Technical Information Service (NTIS) Springfield, Virginia 22151

19. SECURITY CLASS (THIS REPORT) UNCLASSIFIED

21. NO. OF PAGES 44

20. SECURITY CLASS (THIS PAGE) UNCLASSIFIED

22. Price